Reactive Deposition of Metal Thin Films within Porous Supports from Supercritical Fluids

Neil E. Fernandes, Scott M. Fisher, Joseph C. Poshusta, Dionisios G. Vlachos, Michael Tsapatsis, and James J. Watkins*

Department of Chemical Engineering, The University of Massachusetts, Amherst, Massachusetts 01003

Received October 18, 2000. Revised Manuscript Received January 23, 2001

Continuous palladium films were synthesized at controlled depths within porous alumina disks by H_2 reduction of organopalladium compounds dissolved in supercritical CO_2 at 60 °C using an opposing reactants deposition geometry. Film position was controlled by adjusting the relative concentrations of H_2 and the palladium precursor (π-2-methylallyl(cyclopentadienyl)palladium (II) or palladium(II) hexafluoroacetylacetonate) on opposite sides of the alumina substrate. Because of a disparity in the diffusivity of the metal precursor and H_2 in the support, a temporary barrier of poly-4-methyl-1-pentene on the H_2 side of the alumina substrate was used to reduce H_2 flux in a controlled manner. Guided by a simple mass transport model, Pd films between 2 and 80 μm thick were deposited at prescribed depths between 80 and 600 μm as measured from the precursor side. Electron probe microanalysis indicated complete pore filling of the porous alumina at the reaction zone and X-ray diffraction revealed that the structure of the deposit is nanocrystalline. The flux of N_2 through the alumina disk was reduced by over 4 orders of magnitude after deposition and annealing at 500 °C.

Introduction

Thin film metal deposits are of interest for a wide variety of applications involving optics, microelectronics, sensors, membranes, and catalysts. A high degree of control over film quality and position is required when designing advanced materials for specialized applications. One such application is the preparation of supported thin film membranes. In particular, dense palladium metal membranes have application in H_2 recovery and purification and are vital for further development of membrane reactors.[1] Although dense palladium films can offer extremely high selectivity, permeate fluxes are low, and the associated membrane cost is high. Thus, to make practically useful membranes, the permselective films must be very thin, typically on the order of a micrometer. Thin films are also desirable from the standpoint of economy, especially when the film is comprised of a precious metal.

Because micrometer-thick films do not have the mechanical integrity to be freestanding, the ideal membrane is likely to be a composite in which a thin, bicontinuous deposit/substrate zone is located *within* a highly porous matrix. In contrast to films prepared on top of porous substrates (e.g., via electroless deposition or sputtering), membranes prepared by embedding the deposit within the porous matrix offers several benefits. The dense film is protected from incidental abrasion, is less likely to suffer adhesion problems, and especially in the case of precious metals is less expensive—for a commensurate membrane thickness, the percentage of metal used is equivalent to the percentage of support porosity. Moreover, films deposited on top of a substrate must be continuous and defect-free on a large length scale. Because of deposition only inside the porous region, the deposit is required to be defect-free over much smaller length scales. Although its high affinity for H_2 makes Pd the most promising candidate for dense metal membranes,[2] this metal is prone to H_2 embrittlement. Hydrogen embrittlement occurs as a result of lattice stresses induced by the interconversion of the α and β hydride phases at temperatures below 298 °C. Although this problem has traditionally been treated by alloying Pd with various metals (most notably silver (23% Ag), but also nickel (6% Ni) and gold (8% Au)[2]), it has been suggested that Pd, tightly packed into the pores of a supporting matrix, has some resistance toward embrittlement.[3,4]

An elegant method for fabricating such bicontinuous zones is opposing reactants chemical vapor deposition (ORCVD)[5,6] in which chemical reactants are contacted within a porous substrate via an opposing reactants geometry. Reactants diffuse into the porous substrate from opposite faces and react, forming a solid product in a narrow band within the substrate. In principle, any

* To whom correspondence should be addressed. E-mail: watkins@ecs.umass.edu.

(1) Hsieh, H. P. *Inorganic Membranes for Separation and Reaction*; Elsevier: Amsterdam, 1996; Vol. 3.

(2) Shu, J.; Granjean, B. P. A.; Neste, A. V.; Kaliaguine, S. *Can. J. Chem. Eng.* **1991**, *69*, 1036.

(3) Yan, S.; Maeda, H.; Kusakabe, K.; Morooka, S. *Ind. Eng. Chem. Res.* **1994**, *33*, 616.

(4) Jun, C.; Lee, K. *J. Membr. Sci.* **1999**, *157*, 107.

(5) Gavalas, G. R.; Megiris, C. E.; Nam, S. W. *Chem. Eng. Sci.* **1989**, *44*, 1829.

(6) Isenberg, A. O. *Solid State Ionics* **1981**, *314*, 431.

10.1021/cm000837t CCC: $20.00
Published on Web 05/23/2001

remaining porosity or defect allows the direct contact of the reactants, and thus it ensures that a gastight solid layer can be formed. Initial applications of ORCVD have included thin, gastight, oxide films such as yttria-stabilized zirconia (for solid oxide fuel cells[7]), pore plugging with metal deposits in porous oxygen-ion conducting oxides for high flux membranes,[8] dense silica membranes,[9] and more recently, palladium membranes for H_2 separation.[10]

Although a promising technique for infiltrating porous media in theory, the processing difficulty common to all ORCVD methods described to date is the control of the metal precursor vapor phase concentration. Typically, the precursor is a solid or liquid that must be sublimed or evaporated into a carrier gas stream. As a result of solid−liquid−vapor equilibrium, the precursor concentration is typically very low ($\sim 10^{-8}$ mol cm^{-3}), resulting in feed rate limitations. Another concern is the assumption of a precursor-saturated carrier gas stream. The actual vapor phase concentration in the carrier gas stream is often determined by the mass transfer kinetics. Thus, it may not be the case that doubling the carrier gas velocity would double the flux of the precursor. Mixed metal (or oxide) depositions are even more difficult because control over more than one precursor vapor concentration is required.

Here, we describe a novel technique for depositing metal films, which enables *controlled* infiltration and deposition of nanostructured metals and metal alloys within porous substrates using chemical fluid deposition (CFD[11−13]). CFD involves the chemical reduction of a metal organic precursor, which has been dissolved in a supercritical fluid. Instead of relying on sublimation to produce an organometallic vapor, the precursor is dissolved in a supercritical solvent (SCF) such as CO_2. The flexibility of the CFD process arises from the physiochemical properties of the solvent, which lie intermediate to those of liquids and gases. The (gaslike) absence of surface tension enables the SCF to fully infiltrate porous solids and ensures miscibility with gaseous-reducing agents. The (liquidlike) density imparts a solvating power sufficient for maintaining high fluid-phase precursor concentrations while also facilitating ligand desorption from the metal surface after reduction. Moreover, multiple precursors can be simultaneously dissolved, enabling the fluid-phase composition to be tuned to that necessary for a particular alloy composition. Despite being a solution-based technique, the relatively low viscosity, high diffusivity, and miscibility of reagents minimize the mass transport limitations that are usually present in liquid deposition techniques. Thus, CFD can be viewed as a hybrid of CVD and liquid-phase deposition. Although many solvents could be used, CO_2 offers many advantages; it has a convenient critical point (31.1 °C, 73.8 bar), adsorbs only weakly to metal surfaces, is relatively inexpensive, and is environmentally benign. The CFD deposition of Pd, Pt, Ag, Rh, and other metals was recently demonstrated.[12,13] For example, CVD quality palladium films were deposited on patterned silicon wafers and polymer substrates, at 60 °C. This low operating temperature allows the use of organometallics that might otherwise degrade at the high temperatures necessary to generate suitable vapor phase concentrations in CVD.

In this report we demonstrate the controllability that ORCFD imparts to the film fabrication process, by depositing dense palladium films at predetermined locations inside a porous alumina substrate. The controllability of the deposition arises from the ease with which batches of a stable concentrated precursor can be prepared. A mass transfer limited model of ORCFD is derived, which identifies the experimental parameters important for determining the membrane position within the substrate. We utilize the autocatalytic H_2-induced reduction of the metal precursors, π-2-methylallyl-(cyclopentadienyl)palladium (II) (CpPd(π-C_4H_7)) (A) and palladium(II) hexafluoroacetyl-acetonate (Pd(hfac)$_2$) (B);

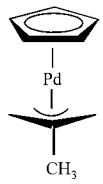

CpPd(π-C_4H_7)

(A)

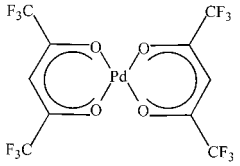

Pd(hfac)$_2$

(B)

however, it should be noted that ORCFD can be used to deposit virtually any metal which has a chemically reducible organometallic form that is soluble in a supercritical fluid.

Mass Transfer Limited Model of ORCFD

Several authors have described the modeling of ORCVD,[14,15] and the extension of the theory to understanding the control of the film deposit (position and thickness) using CFD is relatively straightforward. Following the development of Xomeritakis and Lin,[10] for moderate Thiele moduli, the substrate cross section can be approximated by a series of three separate regions (Figure 1a). Consider a deposition zone confined to region B, where appreciable concentrations of *both* reactants exist. The guiding principle for predicting the film position is that, at pseudo steady state, the reactant fluxes in regions A and C must balance according to the stoichiometry of the chemical reaction. In the limit of an infinitely fast, irreversible reaction occurring in a porous substrate of thickness L, the reaction zone B, becomes infinitesimally thin and the precise position of the reaction zone, Δx (as measured from the precursor

(7) Cao, G. Z.; Brinkman, H. W.; Meijerink, J.; deVries, K. J.; Burggraaf, A. J. *J. Am. Ceram. Soc.* **1993**, *76*, 2201.
(8) Carolan, M. F.; Dyer, P. N.; Fine, S. M.; Makitka, A., III; Richards, R. E.; Schaffer, L. E. Method for manufacturing inorganic membranes by organometallic chemical vapor infiltration. U.S. Patent 5,332,597, 1994.
(9) Tsapatsis, M.; Kim, S. J.; Nam, S. W.; Gavalas, G. R. *Ind. Eng. Chem. Res.* **1991**, *30*, 2152.
(10) Xomeritakis, G.; Lin, Y. S. *AIChE J.* **1998**, *44*, 174.
(11) Watkins, J. J.; McCarthy, T. J. Method of Chemically Depositing Material on a Substrate. U.S. Patent 5,789,027, 1998.
(12) Blackburn, J. M.; Long, D. P.; Watkins, J. J. *Chem. Mater.* **2000**, *12*, 2625.
(13) Long, D. P.; Blackburn, J. M.; Watkins, J. J. *Adv. Mater.* **2000**, *12*, 913.
(14) Tsapatsis, M.; Gavalas, G. R. *AIChE J.* **1992**, *38*, 847.
(15) Xomeritakis, G.; Lin, Y.-S. *Ind. Eng. Chem. Res.* **1994**, *33*, 2607.

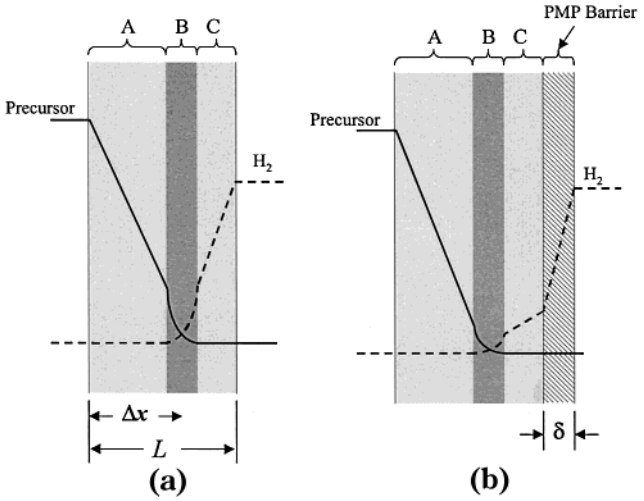

Figure 1. Cross section of opposing reactants deposition zone with precursor and H_2 concentration profiles within a porous support (a) and a support with a PMP barrier layer (b).

side), is found by balancing the diffusive fluxes of reactants in regions A and C

$$\frac{\alpha D_P C_P}{\Delta x} = \frac{D_{H_2} C_{H_2}}{L - \Delta x} \tag{1}$$

where α is a stoichiometric coefficient for H_2 consumption in the reaction. The effective diffusivities of the reactants in the porous substrate are represented by D_i, and with neglect of fluid film resistance, C_i are the respective bulk concentrations of the reactants. The more complicated case of finite reaction rates (low Thiele moduli) requires solution by numerical methods, although semianalytical methods have been proposed.[15]

The amount of H_2 consumed in the reduction of the precursors depends on the degree of hydrogenation that the organic ligands undergo after the initial reduction and deposition of the Pd metal. In batch CFD experiments with an excess of H_2, complete hydrogenation of CpPd(π-C_4H_7) to Pd, cyclopentane, and isobutane was observed.[12] Low-temperature (30−60 °C) CVD studies demonstrated that H_2 reduction of CpPd(C_3H_5) and Pd(C_3H_5)(hfac) produces both saturated and unsaturated products.[16] The difference between these studies is likely due to the low concentration of H_2 in the CVD experiments available for precursor hydrogenolysis and hydrogenation of organic ligands. Because the reaction zone for ORCFD is located where the H_2 and precursor concentrations approach zero, the reduction reaction proceeds under H_2 starved conditions and incomplete hydrogenation of the ligand products may occur.[16] Thus, the H_2 stoichiometry must lie between 1 and 4 for CpPd(π-C_4H_7) and between 1 and 5 for Pd(hfac)$_2$.

Equation 1 can be expressed in the dimensionless form,

$$\Delta\xi = \frac{1}{1+\gamma}, \quad \gamma = \frac{D_{H_2} C_{H_2}}{\alpha D_P C_P} \tag{2}$$

from which it is seen that that the position of the film is controlled by the relative product of the reactant concentrations with their respective diffusivities. One of the difficulties with ORCVD is the disparity between the diffusivities of the bulk precursor and the reductant (H_2), which can differ by 2 orders of magnitude. Because the vapor pressures of organometallic precursors are typically very low, the control of the position of the deposit using ORCVD will be difficult. To control the film position, one must either enhance the diffusivity of the precursor over the reductants or use very low concentrations of the reductant and high concentrations of the metal precursor. In this paper we consider the latter strategy.

In CFD one can obtain precursor concentrations 1000 times greater than in MOCVD; moreover, the low deposition temperature (<100 °C) allows a novel processing route for lowering the reductant concentration. For a typical precursor concentration of 10^{-5} mol cm^{-3}, the mismatch in the diffusivities requires H_2 concentrations on the order of 10^{-7} mol cm^{-3}. Instead of preparing very low concentration H_2/CO_2 mixtures, a more convenient method of controlling the H_2 flux is to use a (temporary) polymer barrier (Figure 1b) that has a low H_2 permeability. In our research, we have opted for a semicrystalline polymer, poly-4-methyl-1-pentene (PMP), ($T_{melt} \sim 230$ °C, $T_{glass} \sim 25$ °C), which at low-pressure conditions has H_2 and CO_2 permeabilities of 3.7×10^{-14} and 2.6×10^{-14} mol m/(m^2 s Pa), respectively.[17] In the presence of supercritical CO_2 at conditions of interest for membrane fabrication, we have measured permeabilities for H_2 through PMP, which are ~15 times higher. Details of this experiment appear later in this paper.

The addition of the polymer barrier alters the analysis of membrane fabrication. By equating the flux of H_2 through the PMP with that in region C (see Figure 1b) and assuming that the reaction only occurs in the porous substrate, the dimensionless position of the reaction zone (again as measured from the precursor side) is obtained.

$$\Delta\xi_{PMP} = \frac{1+\beta}{1+\gamma} \tag{3}$$

$$\gamma = \frac{D_{H_2} C_{H_2}}{\alpha D_P C_P}, \quad \beta = \frac{\delta D_{H_2}}{L D_{PMP}} \tag{4}$$

The addition of the barrier does more than simply reduce the concentration of H_2 at the substrate/polymer interface. The barrier acts as a bottleneck for H_2 transport and breaks the symmetry of eq 2. Thus, if the effective diffusivities of *both* reactants is increased (e.g., by lowering the total pressure or using a more porous substrate), the reaction zone shifts further *inside* the substrate because the parameter β is not a function of only the H_2 diffusivities. Experimentally, for a given substrate and reaction conditions, the position of the film is controlled by the ratio of reactant concentrations and the PMP barrier thickness.

Because Pd is permeable to H_2, even after complete pore blockage, the film continues to grow in thickness. In the early stages of deposition before complete pore blocking, film thickness can be estimated by assuming

(16) Hierso, J.-C.; Satto, C.; Feurer, R.; Kalck, P. *Chem. Mater.* **1996**, *8*, 2481.

(17) Puleo, A. C.; Paul, D. R.; Wong, P. K. *Polymer* **1989**, *30*, 1357.

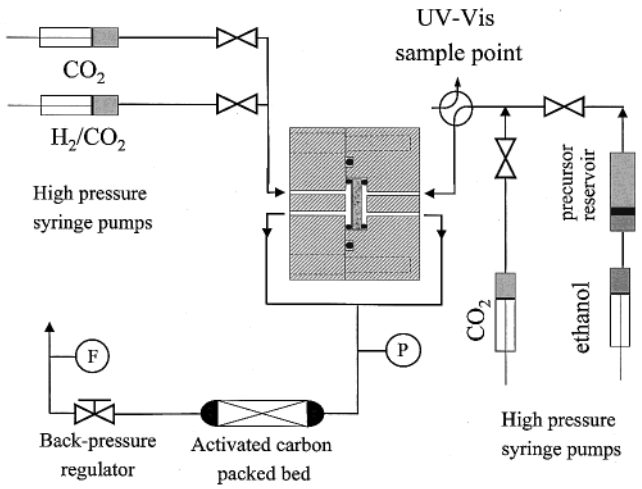

Figure 2. Continuous chemical fluid deposition apparatus for controlled preparation of thin metal films within porous substrates.

a constant rate of deposition and that the Pd deposit has no effect on the H_2 permeation rate such that the deposition front grows toward the precursor side. The mass of Pd deposited, having molecular weight M_{Pd}, is found from integration of the precursor flux ($C_P D_P/\Delta x$) over the reaction time, Δt. Thus, the thickness of the deposit mass is given by

$$\text{thickness} = \frac{C_P D_P}{\Delta x}\Delta t \frac{M_{Pd}}{\rho_{Pd}}\frac{1}{\epsilon} \qquad (5)$$

where ϵ is the substrate porosity and ρ_{Pd} is the deposit density which is assumed to have the value of polycrystalline, dense Pd. As the pores become blocked during late stages of the deposition, the diffusion of H_2 through the nanocrystalline palladium deposit will control the continued growth of the film toward the precursor side and eq 5 no longer holds.

Experimental Methods

Materials. Depositions were performed on porous α-alumina disks prepared by the mechanical compression (5000 lb) of α-alumina powder (Baikowski, CR6), followed by calcination at 1200 °C for 30 h. The resulting disks (diameter 2.1 cm and thickness 0.17 cm) had a porosity of 0.5 with an average pore size of about 0.2 μm as determined by gas permeation measurements and SEM. The 50-μm-thick PMP polymer barrier was obtained from Mitsui Petrochemical of Japan under the trade name TPX with a film grade specification #50 with no finish. High-purity CO_2 and H_2 (Merriam Graves) were used as the solvent and reducing agent, respectively. In this report, we present work using two Pd precursors, π-2-methylallyl(cyclopentadienyl)palladium(II), was synthesized in our laboratory from $[(\pi\text{-}C_4H_7)PdCl]_2$ and cyclopentadienylsodium.[18] The precursor, palladium(II) hexafluoroacetylacetonate, obtained from Aldrich Chemical Co., was sublimed prior to use.

Deposition System. The continuous ORG reactor system is shown in Figure 2. The reactor, precursor reservoir, syringe pumps, and plumbing were constructed of stainless steel, and the temperature of the entire system was controlled at 60 °C. Resistive heating elements heated the reactor, precursor feed cylinder, and associated plumbing, and the syringe pump reservoirs were heated with a water/glycol heating jacket.

The substrate and PMP polymer barrier divided the reactor into separate precursor and H_2 chambers using Buna O-rings to seal the substrate/reactor interfaces. The PMP film has a nominal thickness of 50 μm and is sealed against the alumina support using O-rings. The thickness of the PMP diffusion barrier is readily changed by using multiple layers of PMP. The diffusion of the H_2 through single and multiple layers of PMP has been measured experimentally at reaction conditions: these measurements show no evidence of mass transport limitations between the distinct PMP layers.

High-pressure syringe pumps (Isco 500D) delivered the supercritical fluid streams to their respective reaction chambers at controlled rates. Pressure drop across the support and PMP was minimized by a connection between the precursor and H_2 side outlets where the streams mix. The effluent stream then passed through a carbon bed to adsorb fluid phase reduction products. A backpressure regulator was used to control the system pressure (140 bar).

Deposition Procedure. The H_2/CO_2 solution was prepared by dosing a known amount of H_2 into a CO_2-filled syringe pump to achieve a typical H_2 concentration of 5×10^{-5} mol/cm^3. Concentrations were verified by gas chromatography. The precursor solution was prepared and fed from an external reservoir that was easy to disassemble and clean. This reservoir was a stainless steel tube fitted with an O-ring sealed piston. A syringe pump, containing ethanol, an effectively incompressible fluid, controlled the solution feed rate into the reactor via the piston arrangement (see Figure 2). In a typical deposition experiment, a 1.0×10^{-5} mol/cm^3 precursor solution was prepared in the piston/cylinder by dissolving the appropriate precursor in CO_2 at 138 bar and 60 °C ($\rho \sim 0.55$ g cm^{-3}). A small magnetic stir bar contained in the cylinder provided mixing that ensured uniform precursor distribution within the cylinder prior to depositions.

Initially, the reactor system was pressurized and heated to the desired conditions. A stream of pure CO_2 was passed through the reactor to avoid transient effects of PMP swelling. The pure CO_2 stream was then turned off, and the precursor solution was fed to the reactor typically at a flow rate of 0.3−0.5 cm^3/min. Approximately 30 min was allowed for the precursor to diffuse well within the substrate before the H_2/CO_2 syringe pump metered the reductant to the PMP-covered side of the substrate (typically 0.5 cm^3/min). The mass transfer limited model of deposition predicts deposition to occur within the substrate, but there is no guarantee that this pseudo-steady-state condition can be obtained from arbitrary initial conditions. Feeding the precursor solution to the reactor before administering the H_2 stream assured that the reaction zone started within the substrate as opposed to reacting within the reactor chamber on the precursor side. The precursor concentration was verified throughout the experiment using the sampling technique of McHugh and Paulaitis.[19] A high-pressure liquid sampling valve decompressed a 500-μL sample through a vial containing heptane. Precursor remaining in the sample loop was flushed out with heptane into the vial. The concentration of the resulting precursor/heptane solution was determined by UV−visible absorption spectroscopy.

The duration of deposition was varied between 120 and 220 min depending on the film thickness desired. At shutdown, the H_2/CO_2 flow was first replaced with a flow of pure CO_2. This was required so that the reaction front did not recede from the major deposition zone, as was the case when the precursor flow was shut off first. After ~15 min the precursor flow was also replaced with CO_2 for 15 min after which the system was depressurized slowly.

Because of the novelty of the process, many of the pertinent parameters required for engineering a successful deposition scheme had to be estimated or experimentally determined. Binary diffusivities, $D_{m,i}$, of H_2/CO_2, $Pd(hfac)_2/CO_2$, and $CpPd(\pi\text{-}C_4H_7)/CO_2$ were estimated as 2.6×10^{-3}, 1.3×10^{-4}, and 1.8×10^{-4} cm^2 s^{-1}, respectively, using the method of Fuller et

(18) Tatsuno, Y.; Yoshida, T.; Otsuka, S. *Inorg. Synth.* **1979**, *19*, 220.

(19) McHugh, M. A.; Krukonis, V. J. *Supercritical Fluid Extraction: Principles and Practice*, 1st ed.; Butterworth: Boston, 1986.

al.[20] with a high-pressure correction obtained from the correlation of Takahashi et al.[21] The uncertainty in these estimates is not expected to exceed 20%.[21] Effective diffusivities were estimated using

$$D_i = \frac{\epsilon D_{m,i}}{\tau} \quad (6)$$

where ϵ, the porosity, is 0.5 and τ is an empirical tortuosity taken as 3. A variable volume view cell, as described by McHugh and Krukonis,[19] was used to verify the complete solubility of CpPd(π-C_4H_7) and Pd(hfac)$_2$ at all concentrations used in this work. With a qualitative study of the reduction reaction in the view cell, it was determined that the characteristic time for reaction is much smaller than that required for diffusion in the substrate.

Experimental permeabilities of molecules in polymers under supercritical conditions are not generally available. The method of Wicke−Kallenbach[22] was extended to the measurement of H_2 permeation through PMP films swollen by supercritical CO_2. Differential scanning calorimetry was first used to show that over the time allowed for reaction the PMP crystallinity (31.1%) was not altered by the supercritical solvent. In a diffusion cell very similar to the high-pressure deposition reactor described above, a stream of supercritical CO_2 containing a low concentration of H_2 was passed across one face of the membrane/or substrate while pure supercritical CO_2 was passed over the other face. The pressure difference across the membrane was maintained at zero using a high-precision differential pressure gauge. Because the actual flux across the PMP was small, with knowledge of the volumetric flow rate, F_p, of the permeate stream and measurement (by GC) of the H_2 concentrations in both the retentate (C^R) and permeate streams (C^P), the permeability can be calculated by

$$C^P F_p = D_{PMP} A \frac{(C^R - C^P)}{\delta} \quad (7)$$

where δ is the PMP thickness and A is the available area for diffusion. After the polymer was swelled for approximately 2 h at 60 °C and a CO_2 pressure of 138 bar, D_{PMP} was estimated as 7.2×10^{-6} cm^2 s^{-1}. This estimate corresponds to a permeability of 6.6×10^{-13} mol m/(m^2 s Pa), which is about 18 times greater than the unswollen value of 3.7×10^{-14} mol m/(m^2 s Pa) reported in the literature.[17]

XRD, SEM, and EPMA Characterization. Palladium deposits produced close to the precursor surface were analyzed by X-ray diffraction in a $\theta/2\theta$ geometry (XRD, Philips PW3040-MPD using Cu Kα radiation). The deposit grain size was estimated by analysis of the peak broadening using Scherrer's formula. The depth and density of the Pd deposit was determined by cutting the disks to expose the membrane cross section. Optical microscopy (Olympus BX60) was used to measure the membrane depth and thickness and to determine the uniformity of deposition on macroscopic length scales. Scanning electron microscopy (SEM, JEOL 100CX at 20 kV, substrate lightly coated with gold) and field emission electron microscopy (FEM, JEOL 6320FXV at 5 kV, substrate lightly coated with carbon) were used to further examine the deposit morphology. Electron probe microanalysis (EPMA, Cameca SX-50) was employed to determine the Pd distribution within the substrates and to verify the deposit purity.

Permeation Measurements. Simple N_2 permeance experiments were conducted to ascertain the existence of film defects. The sealing geometry and edge effects impair film formation across the entire width of the substrate. Therefore, ~7-mm-square membrane samples, suitable for permeation measurements, were cut from the center of the composite disk and mounted with TorrSeal high-temperature epoxy to glass slides with a 6.5-mm-diameter bore. The epoxy sealed against the Pd layer by coating the edges (cut faces) of the composite membrane. The glass slide with the attached membrane sample was then mounted with epoxy onto a glass tubular holder.

The preliminary permeation measurements reported here were conducted at temperatures less than 400 K because of thermal limitations of the epoxy. Single-gas N_2 permeances were measured for the membrane-mounted glass tubes in a glass module using the pressure rise method. In this technique, the shell side of the membrane is swept with a pure feed gas at atmospheric pressure and a vacuum is drawn through a calibrated volume on the tube (permeate) side. Prior to the measurement, the membrane is exposed to the pure feed gas and permeate side vacuum for at least 1 h. This time allows gases other than the feed gas to desorb from the membrane and support surfaces. The flow rate through the membrane is determined by determining the rate of pressure increase on the permeate side of the membrane after closing a valve between the vacuum pump and calibrated volume.

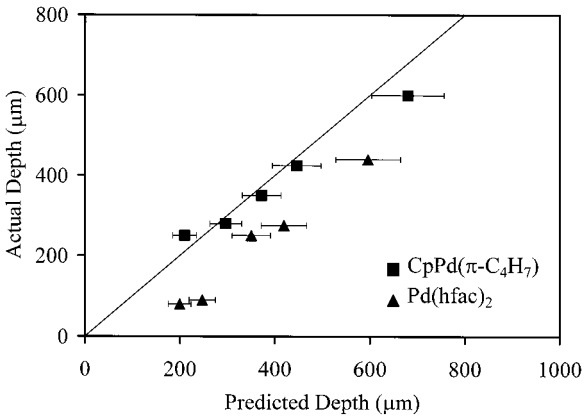

Figure 3. Parity plot of predicted deposit depths vs actual membrane depths. The error bars represent the propagation of diffusivity and concentration errors on the predicted values.

Results and Discussion

Deposit Position and Thickness. Using eqs 3 and 4 as a guide, we fabricated Pd layers at controlled depths in a number of porous alumina supports by varying the PMP barrier thickness and the H_2 and precursor concentrations. These experiments are summarized in Table 1, which describes the type of palladium precursor used and the experimental parameters used to control the deposition. The membrane depths, as measured by optical microscopy of the cross section, ranged from about 80 to 600 μm beneath the precursor-side surface. Membrane depths were not always constant across the diameters of all membrane disks in Table 1 and varied as much as about 10 μm, most likely due to entrance and exit effects in the reactor.

Figure 3 presents a comparison between the deposit depth predictions of eqs 3 and 4 and the actual depths measured using optical microscopy. The stoichiometric coefficients used for H_2 consumed in the reaction were $\alpha = 4$ and $\alpha = 5$ for the reduction of CpPd(π-C_4H_7) and Pd(hfac)$_2$, respectively. The uncertainty of the film depth prediction using eqs 3 and 4 was estimated by propagation of error based on an estimated standard deviation of 5% in the diffusivities and a 1% standard deviation in the reactant concentrations. The error bars in Figure 3 represent one standard deviation in either direction of the predicted membrane position.

(20) Fuller, E. N.; Schettler, P. D.; Giddings, J. C. *Ind. Eng. Chem.* **1966**, *58*, 19.
(21) Reid, R. C.; Prausnitz, J. M.; Poling, B. E. *Properties of Gases and Liquids*, 4th ed.; McGraw-Hill: New York, 1987.
(22) Karger, J.; Ruthven, D. M. *Diffusion in Zeolites*; John Wiley and Sons: New York, 1992.

Table 1. Palladium Membranes Prepared Using ORCFD

membrane	precursor	precursor conc (wt %)	H_2 conc (wt %)	PMP thickness	reaction time (min)	depth from precursor side (μm)
CONP35	CpPd(π-C_4H_7)	0.54	0.44	150	120	600
CONP36	CpPd(π-C_4H_7)	0.53	0.47	100	120	425
CONP39	Pd(hfac)$_2$	0.76	0.61	100	180	80
CONP40	Pd(hfac)$_2$	0.90	0.33	100	200	275
CONP41	Pd(hfac)$_2$	0.87	0.33	50	220	90
CONP46	CpPd(π-C_4H_7)	0.51	0.33	50	195	350
CONP47	CpPd(π-C_4H_7)	0.40	0.33	50	100	280
CONP48	Pd(hfac)$_2$	0.75	0.33	100	195	250
CONP50	Pd(hfac)$_2$	0.88	0.32	150	120	440
CONP54	CpPd(π-C_4H_7)	0.23	0.27	50	200	250

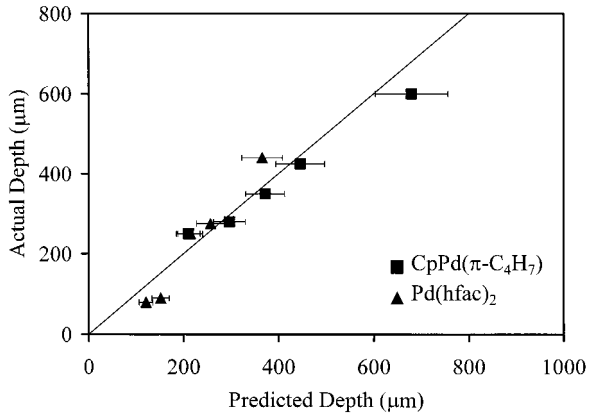

Figure 4. Parity plot of predicted deposit depths with $\alpha = 3$ for the Pd(hfac)$_2$ reduction reaction.

Figure 3 shows good agreement between the predictions of eqs 3 and 4 and the experimental results for the membranes made using the CpPd(π-C_4H_7) precursor. Membranes made with Pd(hfac)$_2$, however, were deposited deeper into the support than predicted by eqs 3 and 4. The precursor dependence of the model's ability to predict the deposit location is probably due to inaccurate estimates of the diffusivities or the assumption that the organic ligands are completely reduced. Smaller H_2 stoichiometric coefficients (e.g., incomplete reduction of the ligands) reduce the predicted depth and cause the Pd(hfac)$_2$ predictions to fall closer to the measured depths as shown in Figure 4 where $\alpha = 3$ was used for the reduction of Pd(hfac)$_2$. Despite possible uncertainty in the precursor diffusivities or stoichiometry, eqs 3 and 4 demonstrate a good ability to predict the membrane position as shown by the linear correlation between the prediction and the measurement. Control of membrane position is demonstrated in Figure 5, which presents optical micrographs for a subset of the membranes described in Table 1. The bright bands are regions of dense Pd while the dark areas do not contain significant Pd deposits (see below).

Figure 6 presents the comparison between the predicted (eq 5 with $\alpha = 3$ for Pd(hfac)$_2$ reduction) and actual membrane thickness for the samples in Table 1. Error bars represent one standard deviation in the membrane thickness based on a 15-min error in reaction run time and using the same estimated errors used for predicting the membrane position. The agreement between the predicted and experimental results did not depend on the type of Pd precursor as did the predicted position (Figure 3). Random error in the deposition thickness may be due to the long-term influences of edge effects and porosity changes with deposition as explained below.

Deposit Microstructure. EPMA scans and optical microscopy cross-section images of samples CONP36 and CONP39 are provided in Figure 7. Figure 7a shows the entire cross section of the substrate used in sample CONP36, whereas Figure 7b focuses on the top 400 μm of the substrate cross section of sample CONP39. From the EPMA results it is clear that the bright bands appearing in the optical microscopy images are regions of high Pd loadings. Given that the porosity of α-alumina is 0.5, one would expect a sample plugged with polycrystalline Pd to contain ~75 wt % Pd. EPMA suggests Pd loadings varying from 40 to 75% in our experiments. EPMA also showed no evidence of fluorine or carbon contamination.

Reaction start-up causes asymmetric distribution of Pd, as evidenced by the dark patterns surrounding the main deposit for CONP36 in Figure 7a. After the initial penetration of the precursor during the first 30 min of the experiment, H_2 quickly permeates the substrate and reduces all of the precursor between the PMP barrier and the reaction zone. The EPMA scans clearly show, however, that the dark zones in the alumina substrates do not contain significant quantities of Pd despite their visibility with optical means. These slight deposits of Pd are consistent with the start-up process employed.

Secondary bands are also visible between about 900 and 1200 μm within the support of membrane CONP36. A pseudo-steady-state model cannot predict such bands, but pressure fluctuations or other experimental instabilities may have caused their formation. While a constant system pressure could generally be maintained by adjusting the back-pressure control valve in Figure 2, sudden drops in system pressure by as much as 4 bar can occur. Indeed, membranes prepared without making adjustments to this valve produced substrates with fewer secondary deposition zones.

As the metal deposition continues at the reaction zone, the porosity of the composite decreases until a dense membrane forms. Figure 8 shows the region of dense deposition in sample CONP39 viewed by scanning electron microscopy. The Pd deposit completely fills the spaces between the sintered alumina particles. Impressions of alumina particles remain visible in the Pd surface exposed by fracturing of the sample. This dense layer prevents the flux of precursor through the porous support, but H_2 can diffuse through the Pd and allow the deposit to continue to grow in thickness. The diffusivity of H_2 in Pd at 60 °C (9×10^{-7} cm^2/s)[23] is about 3 orders of magnitude smaller than that in supercritical

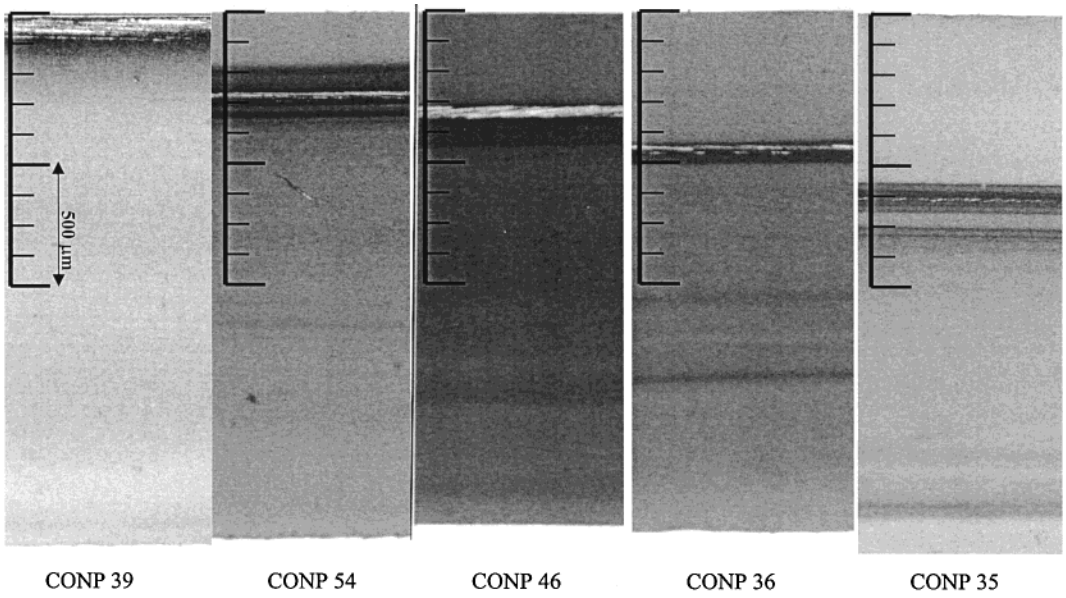

Figure 5. Optical micrographs of five Pd membranes of various thicknesses showing control over Pd film depth (Table 1). The top edge of each micrograph corresponds to the membrane surface on the precursor side of the reactor. The bright bands in each micrograph are dense Pd deposits (see text).

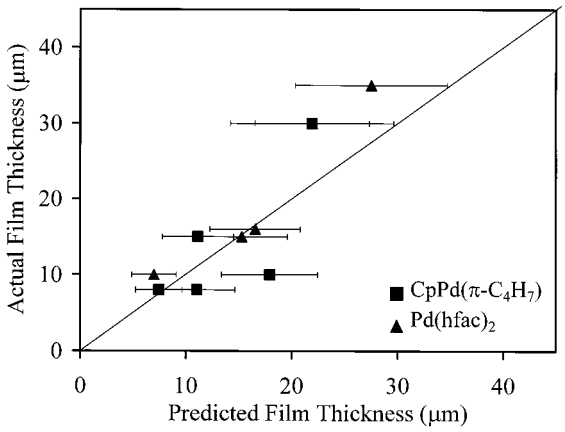

Figure 6. Parity plot of predicted deposit thickness to actual membrane thickness.

CO_2, and therefore the rate of deposition on the precursor side of the Pd membrane is much less than that in the open pores of the bare support. Consequently, any remaining open pores through the Pd membrane provide a region where precursor and H_2 can react and continue to block the pores, ultimately ensuring a continuous Pd layer.

For samples with long reaction times, the deposition around the perimeter of the main deposition zone predicted by eqs 3 and 4 extends from the edge of the predicted membrane zone and curves up to the precursor-side O-ring sealing surface. Since eqs 3 and 4 assume deposition within a slab geometry of infinite area, the deposit formation at the edges of the porous disk cannot be explained by these equations. The infinite slab geometry implies that once the dense membrane forms, membrane growth is limited by the rate of H_2 diffusion through the Pd layer. For the finite disk, however, the dense Pd deposit forms a barrier that redirects reactant diffusion around the membrane edges. For instance, early in the membrane formation, little resistance to transport of reactants is encountered at the reaction zone, and little deposition occurs at the disk edges since transport is largely one-dimensional into the disk. Once the deposit reduces contact between the reactants, the concentrations of reactants on opposite sides of the deposit increase, and they begin to diffuse laterally toward the edges of the disk. Thus, the reaction zone at the edges does not correspond to the predictions of eqs 3 and 4. For the same reasons that ORCFD ensures a defect-free membrane layer, the deposition at the edges continues until a continuous deposit extends from the edge of the predicted membrane zone to the surface O-ring seal.

Deposit Nanostructure. The mechanism of membrane formation suggests that once the dense layer of Pd forms, further membrane growth is mitigated by the small hydrogen diffusivity in Pd metal. Figure 5, however, supports the assumption used to predict thickness by integration of eq 3 over the reaction time, which assumes that the newly formed Pd deposit poses little resistance to H_2 transport and subsequent membrane growth. This discrepancy suggests that the Pd layer remains highly H_2 conductive, allowing continued layer growth after the initial Pd layer is formed. Closer inspection of the membrane nanostructure helps to explain the continued membrane growth.

In sample CONP39 the Pd deposit was sufficiently close to the surface, allowing the collection of the XRD scan as shown in Figure 9. From the Pd(111) peak, the grain size was estimated by Scherrer's method to be ~90 Å, considerably smaller than the average pore size of the α-alumina support. Because the diffusion of hydrogen atoms through crystalline lattices will be much smaller than that through grain boundaries of low packing density, Bryden and Ying,[24] among others, have suggested that the high density of grain boundaries in nanocrystalline materials are conducive to high H_2

(23) Volkl, J.; Alefeld, G. *Diffusion of Hydrogen in Metals*; Volkl, J., Alefeld, G., Eds.; Springer-Verlag: Berlin, 1978; p 321.

(24) Bryden, K. J.; Ying, J. Y. *Mater. Sci. Eng.* **1995**, *A204*, 140.

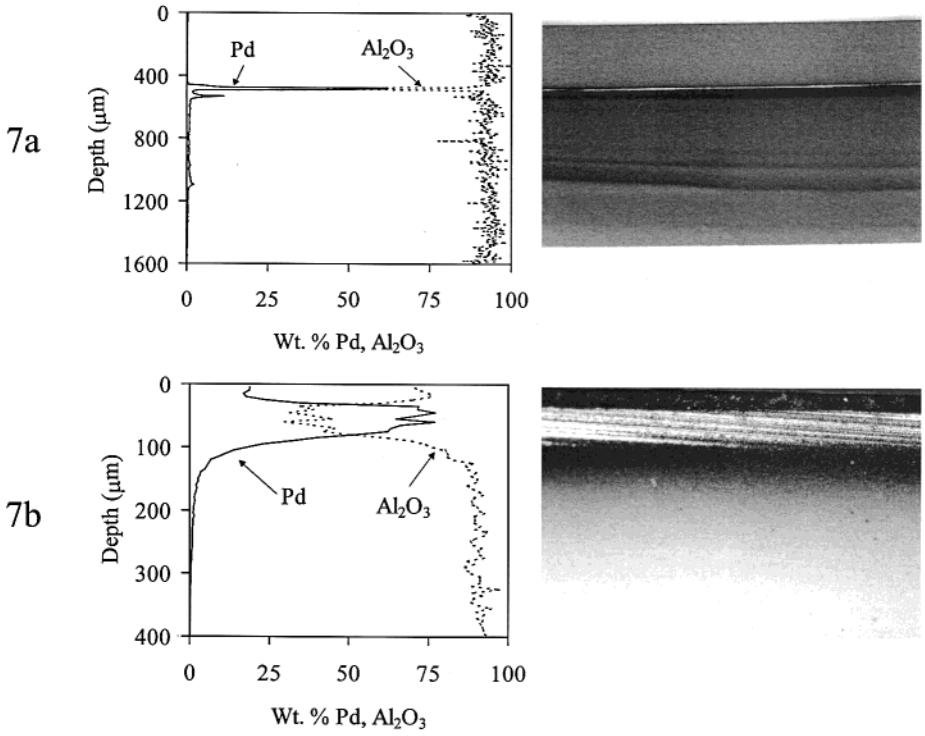

Figure 7. EPMA and optical microscopy cross-section analysis of samples CONP36 and CONP39.

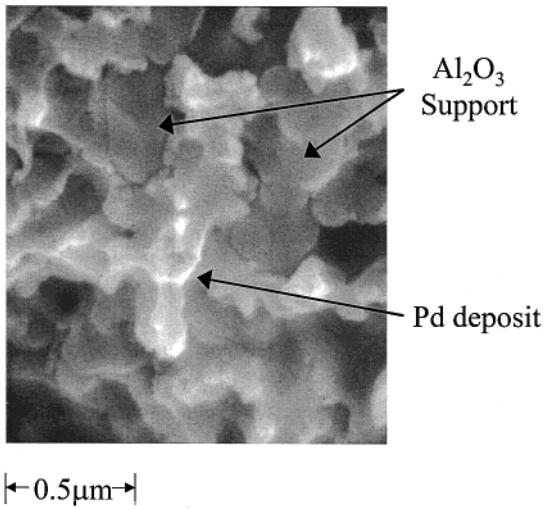

Figure 8. SEM micrograph of the Pd deposit in sample CONP39.

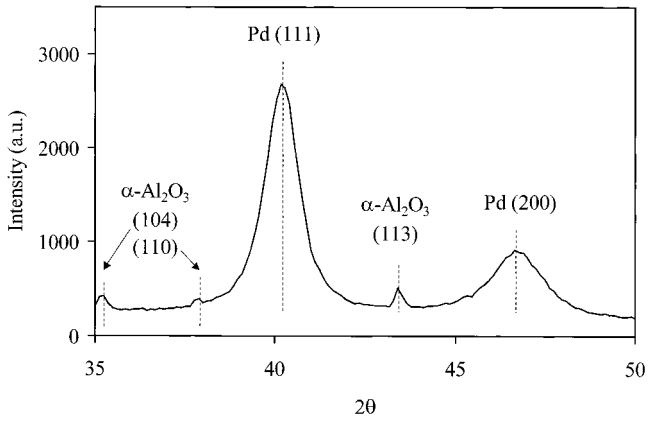

Figure 9. XRD surface analysis of the exposed Pd deposit in CONP39.

fluxes. Indeed, the H diffusivity in nanocrystalline Pd can be 10 times greater than that through dense polycrystalline Pd.[25] The nanocrystalline nature of the deposit also leads us to expect that pore blocking will occur at lower Pd loadings than that required for polycrystalline Pd.

N_2 Permeation Measurements. The moderate agreement between experimental and the membrane thickness and the upper-bound estimate suggest that the nanocrystalline Pd may still be porous to the point where gases other than H_2 can permeate through the grain boundaries and reduce the H_2 selectivity. Indeed, sample CONP36 appeared to have a continuous Pd deposit viewed with optical microscopy, but the N_2 flux was reduced 60 times. The presence of significant N_2 flux suggested that pores exist in the membrane through which N_2 can permeate. Annealing the nanocrystalline composite can reduce grain boundaries by crystal growth and subsequent densification. In fact, we find annealing palladium surface films deposited by CFD for 18 h at 500 °C under a helium atmosphere produced an increase in primary grain size from 80 to 95 Å to 120−130 Å as measured by XRD. Annealing the membranes also significantly reduced N_2 flux. For example, membrane CONP46 was annealed under He at 500 °C for 18 h with 1 °C/min heating and cooling rates. N_2 flux through the annealed sample (7.2×10^{-6} mol/(m^2 s)) was about 26 000 times less than the bare alumina N_2 flux. Membrane CONP39 was also annealed at 500 °C for 18 h and mounted on the glass holder with epoxy. The N_2 flux through this membrane was 3.1×10^{-6} mol/(m^2 s) or about 60 000 times less than the flux through the bare support.

The reduction of N_2 flux through the support indicates that the Pd films prepared by ORCFD were continuous

(25) Kirchheim, R.; Mutschelle, T.; Kieninger, W.; Gleiter, H.; Birringer, R.; Koble, T. D. *Mater. Sci. Eng.* **1988**, *99*, 457.

and dense after annealing, and further investigations on the permeation performance and stability are underway to establish their potential for use as H_2 separation membranes.

Conclusions

Opposing reactants chemical fluid deposition (OR-CFD) proved to be an effective technique for the controlled deposition of nanocrystalline Pd films within porous substrates. The ability to control the location of the Pd membrane is unique to this approach. A steady-state diffusion model identified the important variables required for deposition control and led to a successful continuous deposition process utilizing temporary polymer barriers. Control of the film deposit depth was achieved by manipulating either the thickness of the barrier or the relative concentration of reactants. Electron microprobe analysis and scanning electron microscopy demonstrated that significant amounts of Pd were present in dense films within the substrate. Moreover, single-gas permeation measurements have shown significant reductions in N_2 flux, indicating blockage of the substrate pores in the region of the Pd layer.

Acknowledgment. This work was funded by the National Science Foundation (CTS-9811088). Facilities supported by the Materials Research Science and Engineering Center at the University of Massachusetts were used for deposit characterization. We thank Dr. George Xomeritakis for his assistance with some of the measurements described in the paper.

CM000837T